European Radiology (2019) 29:4133–4140
https://doi.org/10.1007/s00330-018-5832-1

MAGNETIC RESONANCE

Histogram analysis of amide proton transfer–weighted imaging: comparison of glioblastoma and solitary brain metastasis in enhancing tumors and peritumoral regions

Kiyohisa Kamimura[1] · Masanori Nakajo[1] · Tomohide Yoneyama[1] · Yoshihiko Fukukura[1] · Hirofumi Hirano[2] · Yuko Goto[3] · Masashi Sasaki[4] · Yuta Akamine[5] · Jochen Keupp[6] · Takashi Yoshiura[1]

Received: 18 July 2018 / Revised: 17 September 2018 / Accepted: 12 October 2018 / Published online: 28 November 2018

Abstract

Objectives Differentiation of glioblastomas (GBMs) and solitary brain metastases (SBMs) is an important clinical problem. The aim of this study was to determine whether amide proton transfer–weighted (APTW) imaging is useful for distinguishing GBMs from SBMs.

Methods We examined 31 patients with GBM and 17 with SBM. For each tumor, enhancing areas (EAs) and surrounding non-enhancing areas with T2-prolongation (peritumoral high signal intensity areas, PHAs) were manually segmented using fusion images of the post-contrast T1-weighted and T2-weighted images. The mean amide proton transfer signal intensities (APTSIs) were compared among the EAs, PHAs, and contralateral normal appearing white matter (NAWM) within each tumor type. Furthermore, we analyzed APTSI histograms to compare the EAs and PHAs of GBMs and SBMs.

Results In GBMs, the mean APTSI in EAs (2.92 ± 0.74%) was the highest, followed by that in PHAs (1.64 ± 0.83%, $p < 0.001$) and NAWM (0.43 ± 0.83%, $p < 0.001$). In SBMs, the mean APTSI in EAs (1.85 ± 0.99%) and PHAs (1.42 ± 0.45%) were significantly higher than that in NAWM (0.42 ± 0.30%, $p < 0.001$), whereas no significant difference was found between EAs and PHAs. The mean and 10th, 25th, 50th, 75th, and 90th percentiles for APT in EAs of GBMs were significantly higher than those of SBMs. However, no significant difference was found between GBMs and SBMs in any histogram parameters for PHA.

Conclusions APTSI in EAs, but not PHAs, is useful for differentiation between GBMs and SBMs.

Key Points

- *Amide proton transfer–weighted imaging and histogram analysis in the enhancing tumor can provide useful information for differentiation between glioblastomas and solitary brain metastasis.*
- *Amide proton transfer signal intensity histogram parameters from peritumoral areas showed no significant difference between glioblastomas and solitary brain metastasis.*
- *Vasogenic edema alone can substantially increase amide proton transfer signal intensity which may mimic tumor invasion.*

Keywords Glioblastoma · Metastasis · Magnetic resonance imaging

Electronic supplementary material The online version of this article (https://doi.org/10.1007/s00330-018-5832-1) contains supplementary material, which is available to authorized users.

✉ Takashi Yoshiura
yoshiura@m3.kufm.kagoshima-u.ac.jp

[1] Department of Radiology, Kagoshima University Graduate School of Medical and Dental Sciences, 8-35-1 Sakuragaoka, Kagoshima 890-8544, Japan

[2] Department of Neurosurgery, Kagoshima University Graduate School of Medical and Dental Sciences, 8-35-1 Sakuragaoka, Kagoshima 890-8544, Japan

[3] Department of Pathology, Kagoshima University Graduate School of Medical and Dental Sciences, 8-35-1 Sakuragaoka, Kagoshima 890-8544, Japan

[4] Department of Radiological Technology, Kagoshima University Hospital, 8-35-1 Sakuragaoka, Kagoshima 890-8544, Japan

[5] Philips Japan, 13-37, Kohnan 2-chome Minato-ku, Tokyo 108-8507, Japan

[6] Philips Research, Röntgenstraße 24-26, 22335 Hamburg, Germany

Abbreviations

APTSI	Amide proton transfer signal intensity
APTW	Amide proton transfer–weighted
EA	Enhancing area
GBM	Glioblastoma
ICC	Intraclass correlation coefficient
NAWM	Normal appearing white matter
PHA	Peritumoral high signal intensity area
SBM	Solitary brain metastasis

Introduction

Glioblastoma (GBM) and brain metastasis are among the most common malignant brain tumors. Their differentiation is an important clinical problem because the treatment strategy can substantially differ between the two [1, 2]. In some cases, a clinical history of a malignant tumor and/or multiplicity of enhancing brain lesions make the diagnosis of brain metastasis relatively straightforward. However, solitary brain metastasis (SBM) is not uncommon [3], and an SBM may be the first manifestation of disease in 10 to 30% of patients with systemic cancer [4]. On conventional MRI, substantial overlap is present between the findings of GBMs and SBMs. They may show similar signal intensity features both in pre- and post-contrast images. Hence, accurate distinction between GBMs and SBMs can be challenging, often necessitating an invasive surgical biopsy for a definitive diagnosis. Researchers have previously investigated potential roles of advanced MRI techniques such as diffusion-weighted imaging and perfusion imaging for discriminating GBM from SBM [5–7]. However, these methods are not yet established.

Amide proton transfer–weighted (APTW) imaging is a type of endogenous chemical exchange saturation transfer imaging technique [8, 9] that exploits the exchange between amide protons (-NH) in endogenous mobile proteins and bulk-water protons [8]. The APT signal intensity (APTSI) increases with increasing concentration of mobile proteins and peptides in tissue [9–12], although APTSI can be affected by other local factors including temperature and pH. Recent clinical studies have shown that APTW imaging is useful for various aspects of the management of brain tumors including grading of gliomas [11, 13, 14], discriminating tumor recurrence from radiation necrosis [15], and differentiating primary central nervous system lymphoma from glioma [16]. These studies have suggested that APTW imaging can provide unique molecular information that helps characterize brain tumors. Nevertheless, the role of APTW imaging in distinguishing metastatic brain tumors from GBMs has not been established. Therefore, the purpose of this study was to determine whether APTW imaging is useful for distinguishing GBMs from SBMs.

Materials and methods

Study population

The institutional review board of our hospital approved this study, and the requirement for informed consent was waived. From August 2016 to January 2018, 51 patients with pathologically proven GBMs or SBMs underwent MRI including APTW imaging as part of routine pretreatment assessments. Three patients were excluded because they underwent biopsy before MRI. Therefore, 48 patients including 31 with GBM (17 males, 14 females; age range, 11–84 years; mean age, 66.5 ± 14.0 years) and 17 with SBM (9 males, 8 females; age range, 52–88 years; mean age, 65.8 ± 9.0 years) were finally included. No patient underwent treatment, such as surgery, chemotherapy, or radiotherapy, before MRI. Histopathological confirmation was obtained by gross total or partial surgical resection in 43 patients and by stereotactic biopsy in five patients. Primary sites and pathologic diagnoses of SBMs included the lung ($n = 11$; seven adenocarcinomas, two squamous cell carcinomas, one non-small-cell lung carcinoma, one large neuroendocrine carcinoma), colon ($n = 3$, adenocarcinoma), stomach ($n = 1$, adenocarcinoma), kidney ($n = 1$, clear cell carcinoma), and uterus ($n = 1$, endometrioid adenocarcinoma).

MRI

All patients underwent MRI with a 3 T system (Ingenia, Philips Medical Systems) and a 15-channel head coil. On a single axial slice corresponding to the maximum cross-sectional area of the tumor, two-dimensional APTW imaging was performed using a two-channel parallel transmission scheme with a saturation pulse with a duration of 2 s (40 × 50 msec, sinc-gauss-shaped elements) and a saturation power level of $B_{1,\mathrm{rms}} = 2.0$ μT [17, 18] at 25 saturation frequency offsets ranging from -6 to + 6 ppm with a step of 0.5 ppm as well as one far-off-resonant frequency (-1560 ppm) for signal normalization.

The other imaging parameters were as follows: fast spin-echo readout with driven equilibrium refocusing; echo train length = 128; sensitivity encoding factor = 1; repetition time = 3600 msec; echo time = 4.8 msec; matrix = 128 × 128 (reconstructed to 256 × 256); slice thickness = 5 mm, field-of-view = 230 × 230 mm; scan time = 2 min 20 s for one Z-spectrum. A ΔB_0 map for off-resonance correction was acquired separately using a two-dimensional gradient-echo with identical spatial resolution for a point-by-point ΔB_0 correction [17, 18].

For reference, conventional images, including T1-weighted, T2-weighted, fluid attenuation inversion recovery, and contrast-enhanced T1-weighted images were acquired in the axial plane (see Supplementary Table 1).

APTW imaging processing

APTSI is defined as asymmetry of the magnetization transfer ratio at saturation frequency offsets 3.5 ppm: MTR_{asym} (3.5 ppm) [9].

$$\begin{aligned} \mathrm{APTSI} &= \mathrm{MTR}_{\mathrm{asym}}(3.5\ \mathrm{ppm}) \\ &= [S_{\mathrm{sat}}(-3.5\ \mathrm{ppm}) - S_{\mathrm{sat}}(+3.5\ \mathrm{ppm})]/S_0 \end{aligned} \quad (1)$$

where S_{sat} (-3.5 ppm), S_{sat} (+ 3.5 ppm), and S_0 are the signal intensities obtained at -3.5, + 3.5, and -1560 ppm, respectively. All image data were analyzed with the software program ImageJ (v1.47v). A plug-in was created to calculate the MTR_{asym} following correction for B_0 inhomogeneity, using interpolation among the Z-spectral image data.

Image analysis

The post-contrast T1-weighted and T2-weighted images of each patient were co-registered to the source image of the APTW image (an image obtained at 3.5 ppm) with affine transformations using the Turboreg algorithm [19]. The image co-registration was performed to minimize possible effects from misalignment between scans with different dimensions due to patient's minimal head motion. On the fusion image of the post-contrast T1-weighted and T2-weighted images, EA, PHA, and NAWM were manually segmented by two independent neuroradiologists (observer 1 and observer 2 with 3 years of experience each) using the software program ImageJ. Macroscopic cysts and hemorrhagic components were excluded. The segmented regions were copied onto the APTW image (Fig. 1).

APTSI was measured in all pixels included in the segmented region. The mean size of EA, PHA, and NAWM were 637 ± 364 pixels (range 10 to 1469 pixels), 761 ± 761 pixels (range 52 to 3240 pixels), and 171 ± 97 pixels (range 64 to 453 pixels), respectively. Histogram analyses were performed to measure the mean APT and 10th, 25th, 50th, 75th, and 90th percentiles for APT ($APT_{10,\ 25,\ 50,\ 75,\ and\ 90}$) for the EAs and PHAs of each tumor.

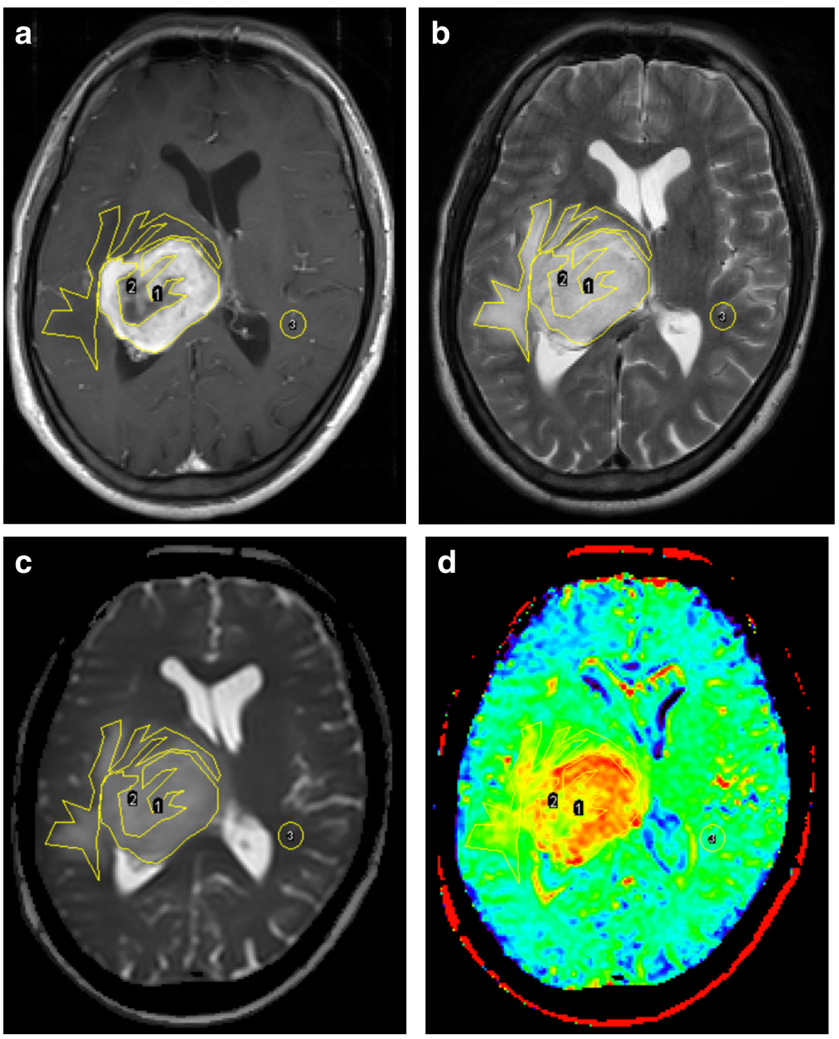

Fig. 1 Segmented enhancing areas and the peritumoral areas in a 57-year-old male with a glioblastoma overlaid onto co-registered post-contrast T1-weighted (**a**), T2-weighted (**b**), APT source (**c**), and APT-weighted (**d**) images. The APT-weighted image shows a marked increase in APT signal in the enhancing area (mean = 3.53%, polygonal ROI 1) and a mild increase in the peritumoral area (mean = 2.04%, polygonal ROI 2) compared to the normal appearing white matter (mean = 0.74%, circular ROI 3)

Statistical analyses

The patients' gender distribution was compared between GBMs and SBMs using the chi-square test, and their mean age was compared using the Mann-Whitney *U* test. The inter-observer agreement regarding the measurements by the two observers was analyzed by calculating the intra-class correlation coefficient (ICC). The measurements by the two observers for each patient were averaged for further analysis. The mean APTSIs were compared among EAs, PHAs, and NAWM within each tumor type using analysis of variance followed by a Tukey Kramer post hoc test. The histogram parameters were compared between the two tumor types for EAs and PHAs using the Mann-Whitney *U* test.

ROC analyses were conducted to evaluate the diagnostic performance of the parameters for differentiating GBMs from SBMs. Statistical analyses were performed with commercially available software packages (SPSS, IBM 19; GraphPad Prism 6, Version 6.07; and MedCalc, Version 15.10.0). *P* values < 0.05 were considered significant.

Results

Comparisons of gender and age distribution

There was no significant difference between the GBMs and SBMs in gender or age distribution ($p = 0.752$ and 0.862, respectively).

Inter-observer agreement

The ICCs of the measurements by the two observers were showed in Table 1. Excellent agreement (ICCs ranging from 0.933 to 0.978) was observed for the mean and $APT_{10,\ 25,\ 50,\ 75,\ and\ 90}$ of the EAs and PHAs in GBMs and SBMs.

Comparisons of APTSI in the EAs, PHAs, and NAWM within each tumor type

Figure 2 shows the comparisons of APTSI in the three ROIs within each tumor type. In GBMs, the mean APTSI in the EAs ($2.92 \pm 0.74\%$) was the highest, followed by that in PHAs ($1.64 \pm 0.83\%$) and NAWM ($0.43 \pm 0.83\%$). A significant difference was observed in each pairwise comparison ($p < 0.001$ each). In SBMs, the mean APTSI in the EAs ($1.85 \pm 0.99\%$) and PHAs ($1.42 \pm 0.45\%$) was significantly higher than that in NAWM ($0.42 \pm 0.30\%$, $p < 0.001$), whereas no significant difference was found between EAs and PHAs ($p = 0.269$).

Table 1 Inter-observer agreement

	ICC
EA	
Mean	0.976
10th percentile	0.976
25th percentile	0.970
50th percentile	0.976
75th percentile	0.971
90th percentile	0.969
PHA	
Mean	0.974
10th percentile	0.933
25th percentile	0.965
50th percentile	0.975
75th percentile	0.978
90th percentile	0.977

ICC intra-class correlation coefficient, *EA* enhancing area, *PHA* peritumoral high signal intensity area

Comparisons of histogram parameters between GBMs and SBMs

Table 2 shows the comparisons of the APTSI histogram parameters between GBMs and SBMs. The mean and $APT_{10,\ 25,\ 50,\ 75,\ and\ 90}$ in the EAs of GBMs were significantly higher than those of SBMs ($p < 0.001$, < 0.001, < 0.001, < 0.001, 0.004, 0.047, respectively). However, no significant

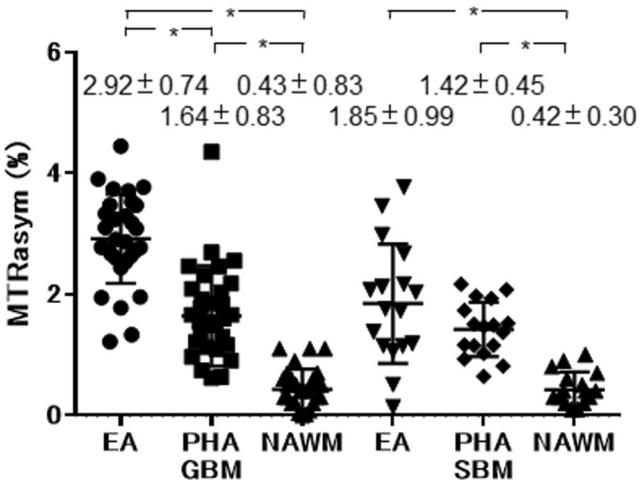

Fig. 2 Comparisons of the mean amide proton transfer–weighted signal intensity (APTSI) measured in the enhancing area (EA), peritumoral high signal intensity area (PHA), and normal appearing white matter (NAWM) for GBMs and SBMs. In GBMs, the mean APTSI in the EAs is the highest, followed by that in PHAs and NAWM, with a significant difference in each pairwise comparison. In SBMs, the mean APTSI in the EAs and PHAs are significantly higher than that in NAWM, whereas no significant difference is shown between EAs and PHAs. The mean ± SD is shown above each plot. *$p < 0.001$. *MTRasym* = asymmetry of the magnetization transfer ratio at saturation frequency offsets 3.5 ppm. Each symbol is one patient

Table 2 Measurements of APT signal histogram parameters in GBMs and SBMs

	GBM ($n = 31$)	SBM ($n = 17$)	p value
EA			
Mean (%)	2.92 ± 0.74	1.58 ± 0.99	< 0.001
10th percentile (%)	1.77 ± 1.17	0.45 ± 1.07	< 0.001
25th percentile (%)	2.33 ± 0.84	1.11 ± 0.86	< 0.001
50th percentile (%)	2.95 ± 0.72	1.84 ± 0.88	< 0.001
75th percentile (%)	3.54 ± 0.94	2.59 ± 1.16	0.004
90th percentile (%)	4.07 ± 1.28	3.26 ± 1.40	0.047
PHA			
Mean (%)	1.64 ± 0.83	1.42 ± 0.45	0.319
10th percentile (%)	0.79 ± 0.91	0.74 ± 0.37	0.819
25th percentile (%)	1.20 ± 0.77	1.09 ± 0.38	0.576
50th percentile (%)	1.62 ± 0.85	1.43 ± 0.46	0.400
75th percentile (%)	2.07 ± 0.97	1.79 ± 0.53	0.275
90th percentile (%)	2.52 ± 1.31	2.10 ± 0.58	0.222

APT amide proton transfer, *GBMs* glioblastomas, *SBMs* solitary brain metastases, *EA* enhancing area, *PHA* peritumoral high signal intensity area

difference was found between GBMs and SBMs in any histogram parameters for PHAs.

Figure 3 demonstrates the histogram profiles over all pixels in the patients as obtained by one of the two observers. Our normalized histogram analysis of the APTSI over all pixels in EA ROIs (GBM: 20,974 pixels, SBM: 9271 pixels) revealed that the overall histogram profile shifted towards a higher APTSI in the GBM group compared with the SBM group. On the other hand, the overall histogram profile of PHA ROIs (21,120 pixels) in the GBM group was similar to that of the SBM group (15,077 pixels).

Diagnostic performance in differentiating GBMs from SBMs

Table 3 summarizes the diagnostic performance of the parameters as determined by ROC analyses. Moderate to high diagnostic performance was achieved by the mean and $APT_{10,\ 25,\ 50,\ 75,\ and\ 90}$ in the EAs, with the area under the curve ranging from 0.70 to 0.85. All parameters of APT histogram analyses of the PHAs resulted in low diagnostic performance.

Figures 1 and 4 show representative cases of GBM and SBM, respectively.

Discussion

The high APTSI in the tumor core of high grade gliomas is a consistent finding among previous studies [11, 14, 20, 21] and has been attributed to abundant mobile proteins and peptides in the proliferating tumor cells. Our finding of increased APTSI in PHAs in GBM relative to NAWM is consistent with a report by Wen et al [11] PHAs in malignant gliomas may

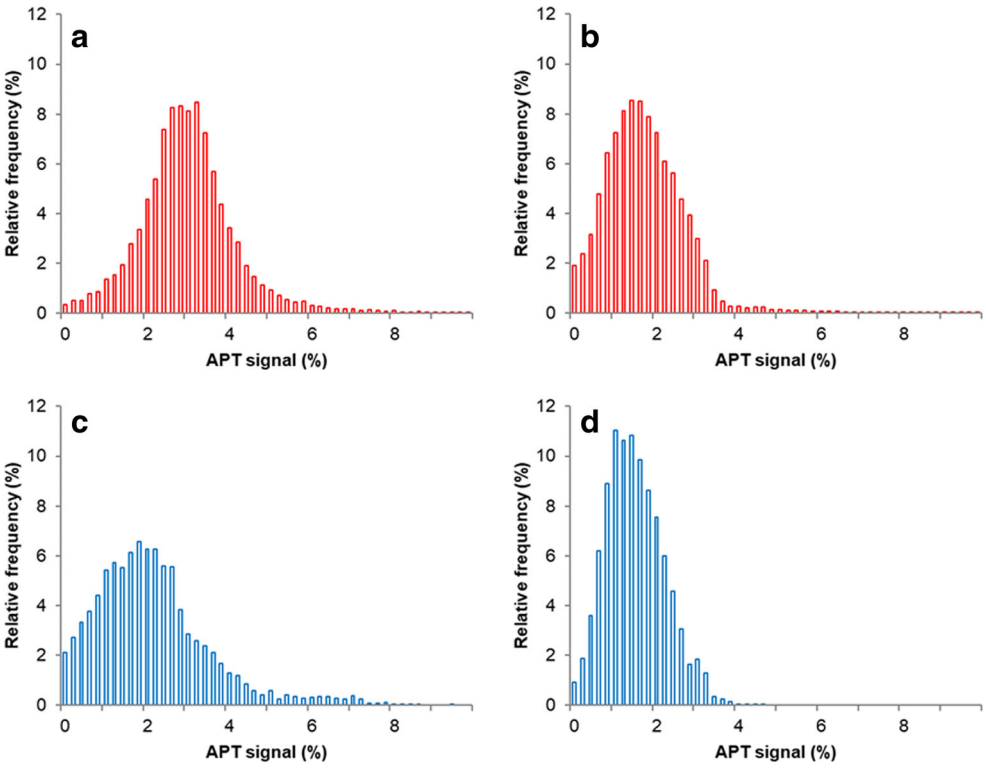

Fig. 3 Histogram profiles over all pixels in enhancing areas (EAs) and peritumoral high signal intensity areas (PHAs) in the patients with glioblastoma (GBM) (**a**, EAs; **b**, PHAs) and those with solitary brain metastasis (SBM) (**c**, EAs; **d**, PHAs). Note that the overall histogram profile for EAs shifts towards the higher APT signal in the GBM group (**a**) compared with the SBM group (**c**), whereas the histogram profiles for PHAs in GBM (**b**) and SBM (**d**) are similar

Table 3 ROC curve analysis for differentiation of GBMs and SBMs

	AUC	Cutoff value (%)	Sensitivity (%)	Specificity (%)	Z-statistics	*p* value
EA						
Mean	0.81	2.17	26/31 (83.9)	13/17 (76.5)	4.15	< 0.0001
10th percentile	0.85	1.65	22/31 (71.0)	16/17 (94.1)	6.19	< 0.0001
25th percentile	0.85	1.80	25/31 (80.7)	14/17 (82.4)	6.30	< 0.0001
50th percentile	0.84	2.20	26/31 (83.9)	13/17 (76.5)	5.35	< 0.0001
75th percentile	0.76	2.80	25/31 (80.7)	12/17 (70.6)	3.20	0.0014
90th percentile	0.70	3.00	27/31 (87.1)	9/17 (52.9)	2.25	0.0246
PHA						
Mean	0.59	1.52	18/31 (58.1)	12/17 (70.6)	1.11	0.2685
10th percentile	0.55	0.90	15/31 (48.4)	13/17 (76.5)	0.65	0.5152
25th percentile	0.55	1.50	10/31 (32.3)	15/17 (88.2)	0.57	0.5672
50th percentile	0.57	1.90	10/31 (32.3)	15/17 (88.2)	0.90	0.3742
75th percentile	0.60	2.50	10/31 (32.3)	16/17 (94.1)	1.21	0.2267
90th percentile	0.59	2.74	11/31 (35.5)	16/17 (94.1)	1.12	0.2616

AUC area under the curve, *GBMs* glioblastomas, *SBMs* solitary brain metastases, *EA* enhancing area, *PHA* peritumoral high signal intensity area

include both tumor infiltration and vasogenic edema. Proteins and peptides associated with infiltrating tumor cells may have contributed to the APTSI in PHAs. In SBMs, the mean APTSI in the EAs and PHAs was significantly higher than that in NAWM. Higher APTSI in PHAs relative to NAWM is consistent with a previous report by Yu et al [22]. Because PHAs in metastatic tumors usually include vasogenic edema without tumor infiltration, these authors speculated that the increased APTSI in PHAs reflects intravascular proteins penetrating into the extravascular space through a leaky blood-brain barrier [22]. In SBMs, unlike in GBMs, the mean APTSI in EAs was not significantly higher than that in PHAs, although the

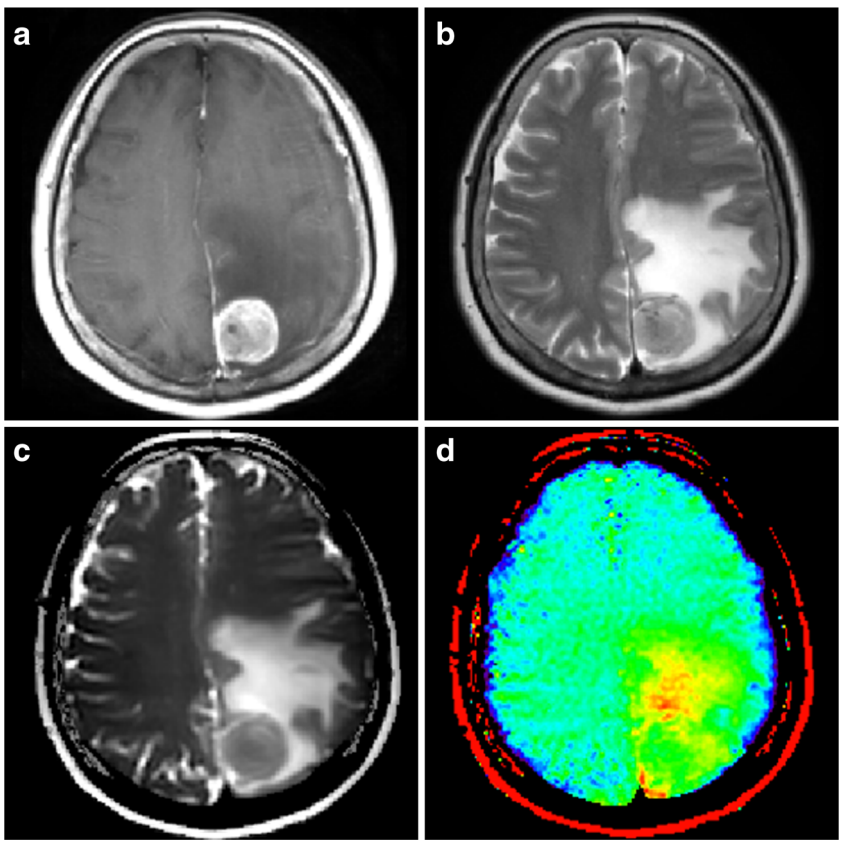

Fig. 4 Images of a 62-year-old female with a metastatic brain tumor from the kidney (clear cell carcinoma). The post-contrast T1-weighted (**a**), T2-weighted (**b**), and APT source (**c**) images show an enhancing mass in the left parietal lobe with extensive peritumoral edema. The APT-weighted image (**d**) shows a mild increase in the APT signal in the enhancing tumor (mean = 1.73%) and a relatively high APT signal in the peritumoral area (mean = 2.08%), compared to the normal appearing white matter (mean = 0.25%)

mean value was slightly higher in EAs. This was unexpected, but APTSI arising from mobile proteins and peptides in the tumor cells of SBMs may not be high enough to dominate mobile proteins and peptides in vasogenic edema.

All APTSI histogram parameters including the mean and $APT_{10,\ 25,\ 50,\ 75,\ and\ 90}$ in the EAs of GBMs were significantly higher than those of SBMs. Moreover, our results suggested that APTSI in EAs may be a promising imaging marker for distinguishing GBMs from SBMs, as demonstrated by ROC analyses. The mechanism for the increased APTSI in GBM compared to SBM is unknown. Because both tumor types can have high cellular density, a difference in cellularity may not be the reason. Additional contribution from protein-rich extracellular matrix filling the extracellular space may explain the high APTSI in GBM [23]. Future comparative studies between imaging and histopathological findings are needed to answer this question.

On the other hand, no significant difference was shown in any of the APTSI histogram parameters obtained from PHAs between GBMs and SBMs. As discussed earlier, PHAs in SBMs likely represent vasogenic edema, whereas those in GBMs may include non-enhancing tumor infiltration. This pathological difference suggests that APTSI in PHAs of GBMs may be higher than that of SBMs, which was not supported by our results. As suggested by the results for SBMs in the report by Yu et al [22] and ours, vasogenic edema alone can substantially increase APTSI. We speculate that APTSI related to edema obscures APTSI from an infiltrating tumor. Our results suggest that APTSI in PHAs may not be an efficient tool for differentiating between GBMs and SBMs. This is in contrast with cerebral blood volume in PHAs derived from MR perfusion imaging, for which the usefulness in discriminating the two tumor types has been demonstrated [6].

To our knowledge, only one previous APTW imaging study has compared GBMs and SBMs. Yu et al [22] reported that APTSI in the peritumoral brain zone of GBMs, which is equivalent to PHAs in our study, was significantly higher than that of SBMs, whereas no significant difference between the two tumor types in APTSI in the enhancing tumor was observed. The discrepant results may be related to different image analysis methods in the two studies. In their study, APTSI was measured in five small (15 pixels) round ROIs placed by two neuroradiologists in consensus. In our study, a histogram analysis was performed by two independent neuroradiologists who traced the contours of EAs and PHAs. Histogram analysis provides higher inter-observer reproducibility than the conventional ROI-based method [24, 25], as supported by the high agreement we obtained. Another possibility is the difference in the APTW imaging pulse sequence, especially in the saturation pulse. Although the two studies share the same pulse strength (2 μT), our study used a longer duration (2 s vs. 0.8 s) to enhance the APT contrast [26]. The method of ATP signal normalization was also different between the two studies. It is possible to acquire S_0 either via switching off radiofrequency (RF) or by far detuning of RF saturation, which essentially yields an unsaturated reference image in either case. In the study by Yu et al [22], an image that did not exert a saturation pulse was acquired for the signal normalization. We assumed that it may be beneficial to use a far detuned RF pulse (-1560 ppm), because the average RF power in the MRI system remains constant during S_0 acquisitions, which may add to the stability of the measured signal. Finally, the heterogeneity of SBM cases in origin, degree of differentiation, and other pathological features may have contributed to the discrepancies. It is possible that discrepant results may be related to smaller sample size in our study that may have led to sampling bias.

The present study has several limitations. First, the cohort was relatively small. The sample size was not large enough to evaluate APTSI of SBMs according to primary sites or pathological types. It should be mentioned that current results, obtained in a population biased towards the SBMs from lung carcinomas, may change when the SBMs from tumors with different pathological types are studied. Second, we did not evaluate the O6-methylguanine-DNA methyltransferase (MGMT) methylation status in our GBMs. The MGMT methylation status could be a strong predictive and prognostic factor in GBMs [27, 28]. Recently, Jiang et al reported that MGMT unmethylated GBMs had higher and more heterogeneous APT-weighted values [29]. Inclusion of MGMT methylation status in future studies would allow a more meaningful comparison. Third, single-slice APTW imaging was employed due to the limited acquisition time in the clinical setting. Use of a three-dimensional sequence with larger coverage may lead to better characterization of heterogeneous tumors and the surrounding tissues. Finally, no histological data were available for PHAs.

In conclusion, APTSI histogram parameters from EAs were significantly higher in GBMs than in SBMs, whereas those from PHAs showed no significant difference between the two tumor types. Our results suggest that APTSI in EAs, but not in PHAs is a useful imaging marker for differentiation between GBMs and SBMs.

Acknowledgments The authors thank Dr. Hajime Yonezawa, MD, PhD, Department of Neurosurgery, Graduate School of Medical and Dental Sciences, Kagoshima University, for providing the clinical information for this article.

Funding The authors state that this work has not received any funding.

Compliance with ethical standards

Guarantor The scientific guarantor of this publication is Takashi Yoshiura.

Conflict of interest The authors of this manuscript declare relationships with the following companies: Jochen Keupp is an employee of Philips Research, and Yuta Akamine is an employee of Philips Japan.

Statistics and biometry No complex statistical methods were necessary for this paper.

Informed consent Written informed consent was waived by the Institutional Review Board.

Ethical approval Institutional Review Board approval was obtained.

Methodology
- Retrospective
- Diagnostic study
- Performed at one institution

References

1. Stupp R, Brada M, van den Bent MJ, Tonn JC, Pentheroudakis G; ESMO guidelines working group (2014) High-grade glioma: ESMO clinical practice guidelines for diagnosis, treatment and follow-up. Ann Oncol 25:93–101
2. Tsao MN, Rades D, Wirth A et al (2012) Radiotherapeutic and surgical management for newly diagnosed brain metastasis(es): an American Society for Radiation Oncology evidence-based guideline. Pract Radiat Oncol 2:210–225
3. Nussbaum ES, Djalilian HR, Cho KH, Hall WA (1996) Brain metastases. Histology, multiplicity, surgery, and survival. Cancer 78: 1781–1788
4. Schiff D (2001) Single brain metastasis. Curr Treat Options Neurol 3:89–99
5. Cha S, Lupo JM, Chen MH et al (2007) Differentiation of glioblastoma multiforme and single brain metastasis by peak height and percentage of signal intensity recovery derived from dynamic susceptibility-weighted contrast-enhanced perfusion MR imaging. AJNR Am J Neuroradiol 28:1078–1084
6. Ma JH, Kim HS, Rim NJ, Kim SH, Cho KG (2010) Differentiation among glioblastoma multiforme, solitary metastatic tumor, and lymphoma using whole-tumor histogram analysis of the normalized cerebral blood volume in enhancing and perienhancing lesions. AJNR Am J Neuroradiol 31:1699–1706
7. Bauer AH, Erly W, Moser FG, Maya M, Nael K (2015) Differentiation of solitary brain metastasis from glioblastoma multiforme: a predictive multiparametric approach using combined MR diffusion and perfusion. Neuroradiology 57:697–703
8. Zhou J, Payen JF, Wilson DA, Traystman RJ, van Zijl PC (2003) Using the amide proton signals of intracellular proteins and peptides to detect pH effects in MRI. Nat Med 9:1085–1090
9. Zhou J, Lal B, Wilson DA, Laterra J, van Zijl PC (2003) Amide proton transfer (APT) contrast for imaging of brain tumors. Magn Reson Med 50:1120–1126
10. Jones CK, Schlosser MJ, van Zijl PC, Pomper MG, Golay X, Zhou J (2006) Amide proton transfer imaging of human brain tumors at 3T. Magn Reson Med 56:585–592
11. Wen Z, Hu S, Huang F et al (2010) MR imaging of high-grade brain tumors using endogenous protein and peptide-based contrast. Neuroimage 51:616–622
12. Togao O, Kessinger CW, Huang G et al (2013) Characterization of lung cancer by amide proton transfer (APT) imaging: an in-vivo study in an orthotopic mouse model. PLoS One Available via https://www.ncbi.nlm.nih.gov/pmc/articles/PMC3797134. Accessed 10 Mar 2018
13. Togao O, Hiwatashi A, Yamashita K et al (2017) Grading diffuse gliomas without intense contrast enhancement by amide proton transfer MR imaging: comparisons with diffusion- and perfusion weighted imaging. Eur Radiol 27:578–588
14. Sakata A, Okada T, Yamamoto A et al (2015) Grading glial tumors with amide proton transfer MR imaging: different analytical approaches. J Neurooncol 122:339–348
15. Mehrabian H, Desmond KL, Soliman H, Sahgal A, Stanisz GJ (2017) Differentiation between radiation necrosis and tumor progression using chemical exchange saturation transfer. Clin Cancer Res 23:3667–3675
16. Jiang S, Yu H, Wang X et al (2016) Molecular MRI differentiation between primary central nervous system lymphomas and high-grade gliomas using endogenous protein-based amide proton transfer MR imaging at 3 Tesla. Eur Radiol 26:64–71
17. Keupp J, Baltes C, Harvey PR, van den Brink J (2011) Parallel RF transmission based MRI technique for highly sensitive detection of amide proton transfer in the human brain at 3T. Proc Intl Soc Mag Reson Med 19:710
18. Togao O, Hiwatashi A, Keupp J et al (2015) Scan-rescan reproducibility of parallel transmission based amide proton transfer imaging of brain tumors. J Magn Reson Imaging 42:1346–1353
19. Thévenaz P, Ruttimann UE, Unser M (1998) A pyramid approach to subpixel registration based on intensity. IEEE Trans Image Process 7:27–41
20. Togao O, Yoshiura T, Keupp J et al (2014) Amide proton transfer imaging of adult diffuse gliomas: correlation with histopathological grades. Neuro Oncol 16:441–448
21. Park JE, Kim HS, Park KJ, Choi CG, Kim SJ (2015) Histogram analysis of amide proton transfer imaging to identify contrast-enhancing low-grade brain tumor that mimics high-grade tumor: increased accuracy of MR perfusion. Radiology 277:151–161
22. Yu H, Lou H, Zou T et al (2017) Applying protein-based amide proton transfer MR imaging to distinguish solitary brain metastases from glioblastoma. Eur Radiol 27:4516–4524
23. Zamecnik J (2005) The extracellular space and matrix of gliomas. Acta Neuropathol 110:435–442
24. Emblem KE, Nedregaard B, Nome T et al (2008) Glioma grading by using histogram analysis of blood volume heterogeneity from MR-derived cerebral blood volume maps. Radiology 247:808–817
25. Law M, Young R, Babb J, Pollack E, Johnson G (2007) Histogram analysis versus region of interest analysis of dynamic susceptibility contrast perfusion MR imaging data in the grading of cerebral gliomas. AJNR Am J Neuroradiol 28:761–766
26. Togao O, Hiwatashi A, Keupp J et al (2016) Amide proton transfer imaging of diffuse gliomas: effect of saturation pulse length in parallel transmission-based technique. PLoS One Available via https://www.ncbi.nlm.nih.gov/pmc/articles/PMC4881971. Accessed 10 Mar 2018
27. Hegi ME, Diserens AC, Gorlia T et al (2005) MGMT gene silencing and benefit from temozolomide in glioblastoma. N Engl J Med 352:997–1003
28. Reifenberger G, Hentschel B, Felsberg J et al (2012) Predictive impact of MGMT promoter methylation in glioblastoma of the elderly. Int J Cancer 131:1342–1350
29. Jiang S, Rui Q, Wang Y et al (2018) Discriminating MGMT promoter methylation status in patients with glioblastoma employing amide proton transfer-weighted MRI metrics. Eur Radiol 28:2115–2123